LWT - Food Science and Technology 139 (2021) 110579

Contents lists available at ScienceDirect

LWT

journal homepage: www.elsevier.com/locate/lwt

High iron bioaccessibility from co-microencapsulated iron/ascorbic acid using chelating polypeptides from brewers' spent grain protein as wall material

Raúl E. Cian [a,*], Janina L. Proaño [a], Pablo R. Salgado [b], Adriana N. Mauri [b], Silvina R. Drago [a]

[a] Instituto de Tecnología de Alimentos, CONICET, FIQ - UNL, 1° de Mayo 3250, (3000), Santa Fe, Argentina
[b] Centro de Investigación y Desarrollo en Criotecnología de Alimentos (CIDCA), CONICET CCT La Plata y Facultad de Ciencias Exactas, Universidad Nacional de La Plata, 47 y 116 S/N°, B1900JJ La Plata, Argentina

ARTICLE INFO

Keywords:
Iron microencapsulation
Brewers' spent grain proteins
Iron bioaccessibility
Spray-drying microencapsulation
Chelating proteins

ABSTRACT

Iron fortification is an important and difficult task since most of the bioavailable iron sources are reactive against food matrix. Microencapsulation technology can prevent iron interaction with food matrix. Co-microencapsulation of iron and ascorbic acid was carried out by spray-drying using a protein concentrate obtained from brewers' spent grain (BSG-PC) and locust bean gum as chelating wall materials. Microcapsules were formulated using a 2^2 factorial design. The effect of BSG-PC/wall material (8.6 and 17.2 g protein 100 g^{-1}) and ascorbic acid/iron molar ratio (0.9:1 and 1.8:1) on iron encapsulation yield (FeE), ascorbic acid encapsulation (AAE), iron chelated by wall material (FeC), iron bioaccessibility (FeB), particle size, zeta potential, and surface hydrophobicity of the microcapsules were assessed. Higher level of BSG-PC increased FeB at low ascorbic acid/iron molar ratio due to the high iron-chelating activity of BSG proteins (IC50: 7.9 ± 1.2 mg mL^{-1}). At low levels of BSG-PC, FeB was promoted by ascorbic acid in a dose response way. A multiple response maximization of FeE, AAE, FeB, and FeC was performed and validated. Optimal microcapsule formula resulted with 29% of FeB after simulated gastrointestinal digestion. The optimization procedure allowed obtaining a fortifier with the higher iron bioaccessibility and iron content.

1. Introduction

Iron deficiency is considered the first nutritional disorder worldwide (Moslemi, Hosseini, Neyestani, Akramzadeh, & Mazaheri, 2018). The main long-term strategy to solve this problem is food fortification. However, the proportion of iron that is absorbed and used in normal body functions (iron bioavailability) is strongly influenced by dietary components (Bryszewska et al., 2019; Yang et al., 2016). In this regard, non-heme iron can interact with several food components during gastrointestinal digestion and form complexes, which can increase or decrease mineral absorption (Lazarte, Carlsson, Almgren, Sandberg, & Granfeldt, 2015). Some compounds, such as phytic acid, can form insoluble complexes with the mineral, hindering its absorption. Conversely, non-heme iron absorption may be enhanced by simultaneous intake of ascorbic acid and animal protein (Hurrell & Egli, 2010). On the other hand, iron is chemically reactive in food matrix and may cause lipid oxidation and/or interact with other food components, affecting the overall nutritive and organoleptic properties of the foodstuff (Moslemi et al., 2018). All these factors make difficult to fortify foods with bioavailable iron sources.

A strategy to protect iron from the interaction with other food components and to increase its release in a specific environment of the gastrointestinal tract is by microencapsulation (Gharibzahedi & Jafari, 2017; Nesterenko, Alric, Silvestre, & Durrieu, 2013). Different studies on iron microencapsulation using low methoxyl pectin, arabic gum, maltodextrin, and resistant starch as encapsulating material have demonstrated that encapsulation increases iron bioaccessibility (Bryszewska et al., 2019; Gupta, Chawla, Arora, Tomar, & Singh, 2015; Moslemi et al., 2014). However, Bryszewska (2019) reported that only 10–30% of encapsulated iron with resistant starch by spray-drying was

Abbreviations: AAE, ascorbic acid encapsulation; **BSG-PC**, protein concentrate obtained from brewers' spent grain; **FeB**, iron bioaccessibility; **FeC**, iron chelated by wall material; and **FeE**, iron encapsulation yield.

* Corresponding author.
E-mail address: rec_704@yahoo.com.ar (R.E. Cian).

https://doi.org/10.1016/j.lwt.2020.110579
Received 7 September 2020; Received in revised form 6 November 2020; Accepted 7 November 2020
Available online 20 November 2020

in ferrous form after simulated gastrointestinal digestion of microcapsules. This result would indicate that iron can undergo oxidation after being released from the encapsulating matrix, affecting its solubility and therefore its bioavailability (Caetano-Silva, Netto, Bertoldo-Pacheco, Alegría, & Cilla, 2020). Note that ferric ion is very poorly soluble at intestinal pH (Palacios, 2012). A current and novel alternative to maintain iron in its ferrous state in the gastrointestinal environment is the use of wall materials with chelating ability such as: proteins, peptides or galactomannans (Caetano-Silva et al., 2020; Hamdani & Wani, 2017). In this sense, complexation with some organic compounds makes iron more stable and less prone to interactions with the chemical environment. Recently, it has been reported that egg yolk proteins with strong chelating capacity used as wall material for the encapsulation of phenolic compounds limit the oxidative damage undergone by active compounds during their transit through the gastrointestinal tract (Sassi, Marcet, Rendueles, Díaz, & Fattouch, 2020). Besides this, the hydrolysis of proteins with chelating capacity by digestives proteases such as pepsin can produce peptides with higher chelating activity than precursor protein (Bamdad, Wu, & Chen, 2011). Regarding galactomannans, it was observed that guar and locust bean gum had ferrous ion chelating ability by forming bridges between iron and the carbonyl groups from gum (Hamdani & Wani, 2017). Recently, Huang, Tao, Li, Zhang, Fan, & Yong (2019) studied the iron bioaccessibility of galactomannan–iron complexes. They found that the iron was easily loosed after gastrointestinal digestion, resulting in iron release rates of 88–94% over 300 min.

Brewers' spent grain (BSG) is the main by-product of the brewing industry with high protein content (Proaño, Salgado, Cian, Mauri, & Drago, 2020). BSG proteins and its peptides have *in vitro* chelating and antioxidant properties such as ferrous ion chelating activity, ferric ion reducing antioxidant power (FRAP), protection against H_2O_2-induced DNA damage, etc. (Bamdad et al., 2011; McCarthy et al., 2013; Proaño et al., 2020; Vieira, Teixeira, & Ferreira, 2016). However, despite having these chelating properties, to date BSG proteins have not been used as mineral encapsulating material. Nor the effect of the addition of another chelating agent to the wall material, such as galactomannans has been studied.

In this context, our working hypothesis is that BSG protein concentrate (BSG-PC), which contains polypeptides with mineral chelating activity, could be used as wall material with reducing and complexing properties, protecting ascorbic acid and maintaining iron in a soluble form. Thus, the aim of this work was to develop microcapsules containing iron and ascorbic acid, with high iron bioaccessibility, using BSG-PC and LBG as chelating wall materials.

2. Materials and methods

2.1. Raw materials and reagents

Brewers' spent grain (BSG) was supplied by Cervecería Santa Fe® (Santa Fe, Santa Fe, Argentina). Locust bean gum Polygum 14/1–125 and maltodextrin 15 DE Globe® 019150 were obtained from Polygum S.C.P® (Sabadell, Barcelona, Spain) and Todo droga (Córdoba, Córdoba, Argentina), respectively. Ferrous sulfate heptahydrate (215422) and L-ascorbic acid (A7506) were obtained from Sigma-Aldrich (Saint Louis, Missouri, USA). Other reagents, of analytical grade, were obtained from Cicarelli Laboratorios (San Lorenzo, Santa Fe, Argentina).

2.2. Brewers' spent grain protein concentrate (BSG-PC)

BSG proteins were extracted by alkaline solubilization (pH 10) during 2 h at room temperature in a pilot plant scale. Solid-liquid separation was performed in a basket type centrifuge with filtering material (2800 rpm and 20 °C) and the supernatant was collected. Then, the supernatant was spray-dried using a Niro Atomizer Spray Dryer (Production Minor®, Copenhagen, Denmark) with an inlet temperature of 170–190 °C and an outlet temperature of 80–90 °C.

The moisture and protein content of BSG-PC were determined using AOAC (1995) methods. Protein content of BSG-PC in dry base was 57.1 ± 0.4 g 100 g^{-1} and moisture content was 4.90 g 100 g^{-1}.

For amino acid analysis, samples of BSG-PC were hydrolyzed with 4 mL of 6 mol L^{-1} HCl in tubes under nitrogen and incubated in an oven at 110 °C for 24 h. Amino acids were determined after derivatization with diethyl ethoxymethylenemalonate by high performance liquid chromatography using a LC-20AT Prominance Liquid Chromatograph (Shimadzu Co., Kyoto, Japan) equipped with a 300 mm × 3.9 mm i.d. reversed-phase column Novapack C18 4 m (Waters®, Milford, Massachusetts, USA) according to the method of Alaiz, Navarro, Giron, and Vioque (1992). Data were processed using Shimadzu LC solution software. Amino acid content was expressed as g/100 g protein. The analysis was performed by triplicate.

Fast protein liquid chromatography (FPLC) of BSG-PC was carried out according to Cian, Garzón, Martínez-Augustín, Botto, and Drago (2018) using an AKTA Prime system equipped with a Superdex peptide column GE Life Sciences® (Piscataway, New Jersey, USA). Elution was monitored at 280 nm and molecular mass was estimated using molecular weight (MW) standards from Pharmacia Fine Chemicals (Piscataway, New Jersey, USA): blue dextran (2000000 Da), cytochrome C (12500 Da), aprotinin (6512 Da), bacitracin (1450 Da), cytidine (246 Da) and glycine (75 Da). The proportion of each molecular species was estimated from FPLC profile, as the rate of the area of each peak by the total area using Origin software version 7.5 (OriginLab®, Northampton, Massachusetts, USA).

Antioxidant properties of BSG-PC were measured by β-carotene bleaching inhibition, reducing power activity, and $ABTS^{\bullet+}$ scavenging capacity, according to Cian, Garzón, Betancur-Ancona, Chel-Guerrero, and Drago (2015).

2.3. Iron chelating activity of wall material components

Iron chelating activity was measured according to Cian, Garzón, Betancur-Ancona, Chel-Guerrero, and Drago (2016). Briefly, 50 μL of samples (BSG-PC, LBG, or MD) were mixed with 50 μL of 8 mg L^{-1} iron solution and incubated 30 min at room temperature. The assay mixture was adjusted to 300 μL with 150 mmol L^{-1} - pH 4.5 acetate buffer containing 0.03 mmol L^{-1} of ascorbic acid. Then, 50 μL of 200 μmol L^{-1} ferrozine solution was prepared and added to assay mixture. The absorbance at 560 nm was measured after 5 min of ferrozine addition. A negative control with 50 μL of 8 mg L^{-1} iron solution +250 μL acetate buffer +50 μL of ferrozine was run. Determinations were carried out in triplicate and the iron chelating activity was calculated as (1):

$$\text{Iron chelating activity (\%)} = [(\text{Abs negative control} - \text{Abs sample})/ (\text{Abs negative control})] \times 100 \quad (1)$$

The concentration causing an iron chelating activity of 50% (IC_{50}) was determined using serial dilutions of samples (BSG-PC, LBG, or MD) from 0 to 50 mg mL^{-1}. The experimental data was fitted using Origin software version 7.5 (OriginLab®, Northampton, Massachusetts, USA) with the following equation (2):

$$y = a - b*c^{x} \quad (2)$$

Where: y, is the inhibition rate, a, b, and c are the regression parameters, and x is the BSG-PC, LBG, or MD concentration (mg mL^{-1}). The IC_{50} value was obtained as (3):

$$IC_{50} = \ln [(50-a)/b]/\ln c \quad (3)$$

All determinations were performed by triplicate.

2.4. Preparation of microcapsules

For co-microencapsulation of iron and ascorbic acid, BSG-PC, LBG,

and MD were used as encapsulating material. Before the spray drying process, BSG-PC, LBG, and MD were added directly to iron/ascorbic acid aqueous solution and stirred during 30 min at room temperature. Such dispersions containing 0.45–1.7 g of iron 100 g^{-1}, 11 g of LBG 100 g^{-1}, and 13 g 100 g^{-1} total solids (Table 1) were dried using a Mini Spray Dryer Büchi B-290 (Büchi Labortechnik AG, Flawil, Switzerland) equipped with an atomizer nozzle of 700 μm diameter. The dispersions were fed into the main chamber through a peristaltic pump and the feed flow rate was controlled by the pump rotation speed (3.1 mL min^{-1}). Drying air flow rate was 357 L h^{-1} and compressor air pressure was 6–8 bar. Inlet and outlet air temperature were 120 ± 2 °C and 48 ± 8 °C, respectively.

A 2^2 factorial design, with three replicates in the central point resulting in 7 runs, was used to study the simultaneous effect of BSG-PC/wall material (8.6 and 17.2 g protein 100 g^{-1}) and AA/Fe molar ratio (0.9:1 and 1.8:1) on iron encapsulation yield (FeE), ascorbic acid encapsulation (AAE), iron chelated by wall material (FeC), iron bioaccessibility (FeB), particle size, zeta potential and surface hydrophobicity of the different microcapsules.

The resulting microcapsules were stored at −20 °C until analysis. Two replicates were assayed for each formula.

The solids and protein content of feed dispersions were determined using AOAC (1995) methods. Iron content of feed dispersion was measured by atomic absorption spectroscopy after wet mineralization. Samples were digested by microwave using a Milestone START D digester (Shelton, Connecticut, USA). A 300-Perkin Elmer Spectrometer (PerkinElmer®, Norwalk, Connecticut, USA) was used. Ascorbic acid content of feed dispersion was determined according to the method of Van de Velde, Pirovani, Cámara, Güemes, and Bernardi (2012), using a Shimadzu Series LC-20AT pump, with Shimadzu SPDM20A diode array detector, equipped with a 250 × 4.6 mm i.d. reversed-phase column (Novapack C18, 5 μm; Gemini 110A C-18 Phenomenex column). Data were processed using Shimadzu LC solution® software (Shimadzu Co., Kyoto, Japan). Iron and ascorbic acid content were expressed as g 100 g^{-1} solid. All determinations were performed by triplicate.

2.5. Characterization of microcapsules

The moisture, protein, iron, and ascorbic acid content of microcapsules were determined as mentioned before. All determinations were performed by triplicate.

Iron encapsulation yield (FeE) was calculated as the ratio between iron content of microcapsules (g) and iron content of feed dispersions (g). Ascorbic acid encapsulation (AAE) was calculated as the ratio between ascorbic acid content of microcapsules (g) and ascorbic acid content of feed dispersions (g).

A scanning electron microscopy (SEM) was performed. Powders were mounted on aluminum stubs using a double-sided tape and were coated with a thin gold layer using a cool sputter system (SCD 005, BAL–TEC, Switzerland). SEM images were acquired with a scanning electron microscope SEM 505 (Philips®, Amsterdam, Netherlands) under high vacuum with a 20 kV acceleration voltage. Morphology of microcapsules was observed with magnifications of 1000 × and the mean particle size of microcapsules was determined using ImageJ® software (National Institutes of Health, Bethesda, Maryland, USA).

Surface hydrophobicity of microcapsules was determined according to Molina-Ortiz et al. (2009). Briefly, microcapsules were dispersed at 0.05 g protein 100 g^{-1} in 10 mmol L^{-1} pH 7.0 potassium phosphate buffer. Five serial dilutions of the sample from 0.05 to 0.005 g 100 g^{-1} protein were made. Then, 10 μL of 8 mmol L^{-1} of 8-aniline-1-naphthalensulphonate (ANS) solution were added to 2 mL of each sample. The fluorescence was measured at excitation wavelength of 390 nm and emission wavelength of 468 nm using a Hitachi 2000 fluorescence spectrophotometer (Hitachi Ltd., Tokyo, Japan). Surface hydrophobicity was calculated according to Cian, Salgado, Mauri, and Drago (2020). Measurements were carried out in triplicate at room temperature.

Zeta potential of microcapsules was determined according to Cian et al. (2020). A dynamic light scattering and micro-electrophoresis instrument Zetasizer Nano ZS90 (Malvern Instruments Ltd., Worcestershire, United Kingdom) was used. All determinations were performed by triplicate.

To estimate the iron chelated by the wall material (FeC), microcapsules were dispersed in bidistilled water at 8 mg iron/L (total iron content). Then, free iron content of dispersion was determined. For this, 40 μL of sample were mixed with 200 μL of 150 mmol L^{-1} pH 4.5 acetate buffers, containing 0.03 mmol L^{-1} of ascorbic acid. A 200 μmol L^{-1} solution of ferrozine was prepared and 40 μL were added to assay mixture. The absorbance at 560 nm was measured at 5 min after ferrozine addition. A negative control with 40 μL of bidistilled water +200 μL acetate buffer +40 μL of ferrozine was run. To estimate the free iron content, an iron calibration curve (0–10 mg L^{-1}) was used. Determinations were carried out in triplicate and FeC was calculated as (4):

$$\text{FeC (\%)} = [(\text{Total iron content} - \text{Free iron content}) / \text{Total iron content}] \times 100 \quad (4)$$

Iron bioaccessibility (FeB) of microcapsules was determined according to the method developed by Miller, Schricker, Rasmussen, and Van Campen. (1981) and modified by Drago, Binaghi, and Valencia (2005). This method measures mineral dialyzability under controlled pH conditions after a digestion-simulating physiological process. Briefly, microcapsules were prepared to 10 g solid 100 g^{-1} dispersion, using deionized water. Aliquots (25 g) of homogenized samples were adjusted to pH 2.0 with 4 mol L^{-1} of HCl and then 0.8 mL pepsin (16 g 100 mL^{-1} pepsin solution in 0.1 mol L^{-1} HCl) were added to digestion mixture and incubated at 37 °C for 2 h in a shaking water bath. In order to adjust the pH during the digestion and dialysis stage, and to obtain an uniform final pH (6.5 ± 0.2) in digest/dialysate systems, a 0.15 mol L^{-1} PIPES buffer with pH varying according to the matrix was used. At the end of pepsin digestion, dialysis bags (cut off: 6–8 kDa) containing 20 mL PIPES

Table 1
Factorial design responses for particle size, iron encapsulation yield (FeE), ascorbic acid encapsulation (AAE), iron chelated by wall material (FeC), iron bioaccessibility (FeB), zeta potential and surface hydrophobicity of the different microcapsules.

Factor Levels	Factors		Particle size (μm)	FeE (%)	AAE (%)	Zeta potential (mV)	FeC (%)	FeB (%)	Surface hydrophobicity
	BSG-PC/wall material (%)	AA/Fe							
−1/1	8.6	1.8	7.4	90.4	64.5	−6.3	24.7	29.3	58.2
−1/-1	8.6	0.9	9.5	97.8	68.6	−6.7	22.6	15.5	43.1
0/0	12.9	1.35	10.8	92.0	64.1	−10.7	31.5	28.2	80.9
0/0	12.9	1.35	10.1	92.1	66.2	−10.5	29.8	25.0	72.4
0/0	12.9	1.35	10.6	93.2	67.0	−8.6	36.8	26.9	79.0
1/1	17.2	1.8	10.4	89.4	78.9	−20.1	59.7	29.7	86.0
1/-1	17.2	0.9	12.9	94.5	65.3	−19.6	50.8	30.7	79.2

BSG-PC/wall material (%): proportion of brewers' spent grain protein concentrate respect to total encapsulating material (g 100 g^{-1} encapsulating material). **AA/Fe**: Ascorbic acid/iron molar ratio. The polynomial equation of prediction was: $y = a_0 + a_1$ BSG-PC/wall material (%) $+ a_2$ AA/Fe $+ a_3$ BSG-PC/wall material (%) x AA/Fe and the corresponding regression coefficients were: a_0, a_1, a_2, and a_3.

buffer were placed in each flask and were incubated for 50 min in a shaking water bath at 37 °C. Then, 6.25 mL of bile pancreatin solution (2.5 g 100 mL^{-1} bile and 0.4 g 100 mL^{-1} pancreatin in 0.1 mol mL^{-1} $NaHCO_3$) were added to each flask and the incubation continued for another 2 h. Then, the content of each dialysis bag (dialysates) was weighed and analyzed regarding mineral content. FeB was calculated as the amount of iron dialysated expressed as a percentage of total iron content in the microcapsule (5):

$$\text{FeB (\%)} = (\text{mg FeD / mg FeM}) \times 100 \quad (5)$$

Where: mg FeD is mg of iron dialysated and mg FeM is mg of iron of microcapsules.

Iron content in the dialysate was measured by atomic absorption spectroscopy after dry mineralization. Ash was removed with 20% HCl (v/v). A 300-Perkin Elmer Spectrometer (PerkinElmer®, Norwalk, Connecticut, USA) was used.

2.6. Optimization and model validation

Derringer's desirability function was used for multiple response optimizations according to Derringer and Suich (1980). The method involves transformation of each predicted response to a dimensionless partial desirability function (*di*). The global desirability function (D) is defined as the geometric mean of the different di values. A value of D different from zero implies that all responses are in a desirable range simultaneously and, consequently, for a value of D close to 1, the combination of the criteria is globally optimal. In this work, FeE, AAE, FeB, and FeC were maximized.

For model validation, microcapsules were obtained by triplicate in the same way as it was previously described using BSG-PC/wall material and AA/Fe molar ratio given by the optimization procedure. The experimental data (FeE, AAE, FeB, and FeC) were compared to values of these responses predicted by the model using a *t*-test analysis.

2.7. Statistical analysis

STATGRAPHICS Centurion XV 15.2.06 (Statpoint Technologies, Inc., Warrenton, Virginia, USA) was used to perform ANOVA, to fit the polynomial equations of experimental data and to obtain the coefficients of such equation. The significance of each term of the models was evaluated referred to pure error. For verification of the model adequacy, the lack of fit and the coefficient of determination (r^2) were calculated. This software was used as well for the numerical optimization procedure through the Derringer's desirability function. The statistical differences among samples were determined using the least significant difference (LSD) test with a level of signification $\alpha = 0.05$.

3. Results and discussion

3.1. BSG-PC characterization and iron chelating activity of wall material components

According to FPLC gel filtration profile, BSG-PC presented three main peaks: >70000 Da, 2900 Da, and 100 Da (Fig. 1A). The components higher than 70000 Da presented an elution volume higher than that corresponding to exclusion volume. The peaks of 2900 Da and 100 Da could correspond to intermediate MW species and free amino acids, respectively. Fig. 1B shows the proportion of different molecular weight specie of BSG-PC respect to total area obtained from FPLC gel filtration. BSG-PC had a high proportion of 2900 Da protein components, while the proportion of high MW species (>70000 Da) and free amino acids (100 Da) was significantly lower ($p < 0.05$). These results suggest that BSG-PC is composed mainly by polypeptides. Cian et al. (2018) showed that alkaline conditions promoted the solubilization of proteins and oligopeptides. Moreover, McCarthy et al. (2013) reported that MW distribution profiles of BSG protein rich isolate had up to 32% of peptides lower than 5000 Da.

Regarding amino acid profile of BSG-PC, the most abundant amino acids were Glu + Asp, His, and Leu (Fig. 1C). Similar amino acid profile was found for brewers' spent grain protein hydrolysates obtained with different enzymatic systems (Cian et al., 2018). Note that the main proteins in BSG are hordeins (60%), which has high content of Glu. Moreover, the barley cell wall structural proteins contain high levels of Asp residues (Conolly, Piggott, & FitzGerald, 2014). On the other hand, proportion of hydrophobic amino acids (Gly, Ala, Val, Leu, Ile, Met, Phe, and Pro) in BSG-PC exceeded 47% (Fig. 1C), which could be associated with the extraction of hordeins fractions, γ-hordein being the most hydrophobic subunit (Celus, Brijs, & Delcour, 2007; Vieira et al., 2014).

BSG-PC presented high antioxidant capacity measured by β-carotene bleaching inhibition (22.81 ± 1.49%), reducing power activity (153.3 ±

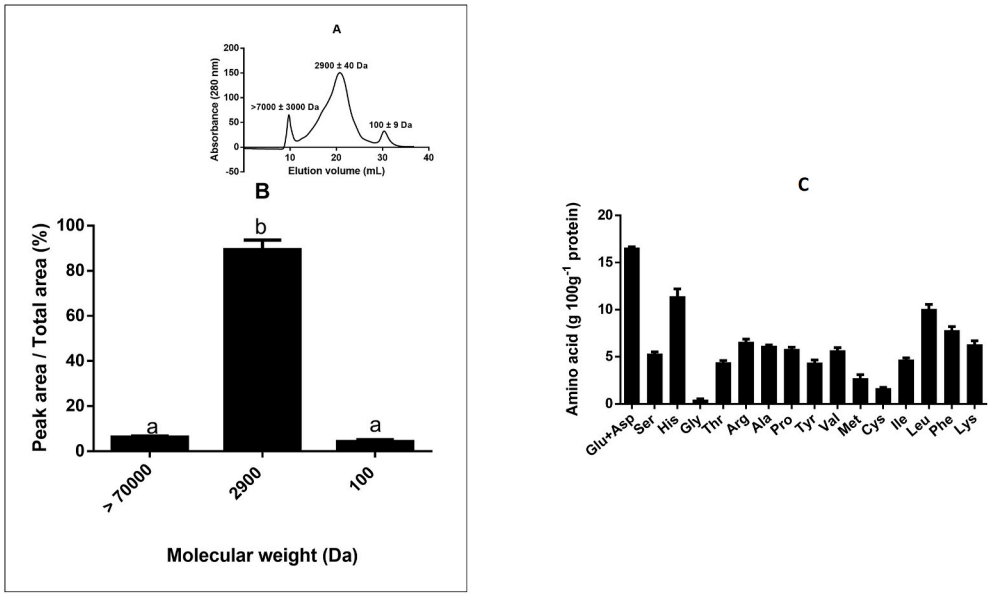

Fig. 1. FPLC gel filtration profiles of BSG-PC (**A**). Proportion of molecular weight species respect to total area obtained from FPLC gel filtration (**B**). The profile is representative of three replicates. Amino acid profile of BSG-PC (**C**).

0.9 mg AA equivalent g^{-1}), and ABTS scavenging capacity (245.2 ± 1.5 μmol Trolox g^{-1}), similar to those described by Vieira et al. (2016) and McCarthy et al. (2013).

Among wall materials, BSG-PC showed the lowest IC_{50} value for iron-chelating activity (Fig. 2A). The high iron-chelating activity of BSG-PC may be due to polypeptide size (high proportion of 2900 Da components) and high content of Glu + Asp residues. Bamdad and Chen (2013) reported that the fraction with MW < 5000 Da obtained from barley hordein hydrolysates had higher iron-chelating activity than that of MW > 5000 Da. In this regard, Bamdad et al. (2011) reported that a limited hordein hydrolysis produce to more amphoteric and structurally flexible polypeptides, capable of entrapping ions. On the other hand, Lv et al. (2009) found that iron-chelating oligopeptides from soybean protein hydrolysates bind to minerals through the acid residues of Glu + Asp. As carboxyl residues of these amino acids have a negative charge at pH > 4.25, their corresponding polypeptides acquires a high chelating capacity of minerals (Caetano-Silva et al., 2020; Cian et al., 2016). Note that in this work the pH of iron-chelating activity assay was 4.5. Torres-Fuentes, Alaiz, and Vioque (2011) reported that a high His content in peptide sequence (around 20–30%) provides high chelating capacity to peptides. As mentioned before, the second most abundant amino acid in BSG-PC was His (Fig. 1C), which could be involved in the chelating ability of polypeptides.

LBG also exhibited iron-chelating activity, obtaining an intermediate IC_{50} value (Fig. 2A). Similar results were reported for methanolic extracts of LBG (Hamdani & Wani, 2017). Some natural polysaccharides have been found to bind divalent ions by forming cross bridges through their carbonyl functional groups (Wang, Chang, Inbaraj, & Chen, 2010). Moreover, Roman, Decker, and Goddard (2015) reported that galactomannans may complex metals by 2 *cis*-hydroxyl groups of each monomeric unit. On the other hand, MD presented the lowest iron-chelating activity (Fig. 2A). This polymer was mainly used as filling agent in the present study due to their excellent encapsulating properties.

3.2. Iron and ascorbic acid co-microencapsulates

Table 1 shows iron encapsulation yield (FeE), ascorbic acid encapsulation (AAE), iron chelated by wall material (FeC), iron bioaccessibility (FeB), particle size, zeta potential and surface hydrophobicity of microcapsules obtained at different proportion of BSG-PC/wall material and AA/Fe molar ratio. Table 2 shows the degree of significance (*p* values) corresponding to each polynomial term of the regression model. Regression models can be considered adequate to describe the effects of **BSG-PC/wall material** and **AA/Fe** on each response since the lack of fit was not significant ($p > 0.05$), and the coefficient of determination (r^2) was acceptable for each one.

The mean size of microcapsules ranged 7.4–12.9 μm (Table 1). These values were within the range expected for microcapsules produced by spray drying (1–50 μm) (Nesterenko et al., 2013). The ANOVA results showed that independent variables were significant ($p < 0.05$). Size of microcapsules was directly related to BSG-PC/wall material and inversely related to AA/Fe molar ratio. Thus, an increase in iron content increased the size of microcapsules. A similar effect was found by Churio and Valenzuela (2018), where an increase of ferrous sulfate respect to encapsulating material (from 1:10 to 1:2.5) increased the mean size of microcapsules obtained by spray drying.

Regarding surface morphology, all microcapsules presented round external surfaces and some concavities (data not shown), which is attributed to mechanical atomization, uneven shrinkage forces due to the rapid evaporation of the droplets by inlet hot air, and cooling solidification involved in spray-drying (Mohan, Rajendran, He, Bazinetc, & Udenigw, 2015; Norkaew et al., 2019; Xie, Wan, Lu, & Hui, 2010). Rapid cooling generates dents due to the wall material shrinkage, especially at high drying rates (Xie et al., 2010). It is important to note that no fissures, cracks, or disruptions were observed in surface morphology of microcapsules. This is fundamental for guaranteeing lower permeability of gases, higher protection and core retention (Oliveira, Moretti, Boschini, Baliero, Freitas, & Favaro-Trindade, 2007). Molina-Ortiz et al. (2009) reported that the use of soybean protein isolates as wall material for microencapsulation of casein hydrolyzates allow obtaining a harder structure of the microcapsules. Moreover, the authors related the structure observed without cracks or disruptions to the good film-forming properties of soybean proteins. In this regard, Proaño et al. (2020) developed active films with BSG protein concentrate using polyethylene glycol as plasticizer. They concluded that BSG proteins could be a cheap alternative for the preparation of biodegradable films with good film-forming properties. On the other hand, it has been reported that proteins improved the surface smoothness and decreased the surface indentation of maltodextrin-based microcapsules. Moreover, it has been observed that combinations of proteins such as whey protein isolates (WPI) with high-DE carbohydrates limit the formation of microcapsule surface dents (Xie et al., 2010).

Regarding FeE, values ranged 89.4–97.8%, and no effect was observed for BSG-PC/wall material proportion ($p > 0.05$). However, FeE was inversely related to AA/Fe molar ratio ($r^2 = 0.9180$). The highest

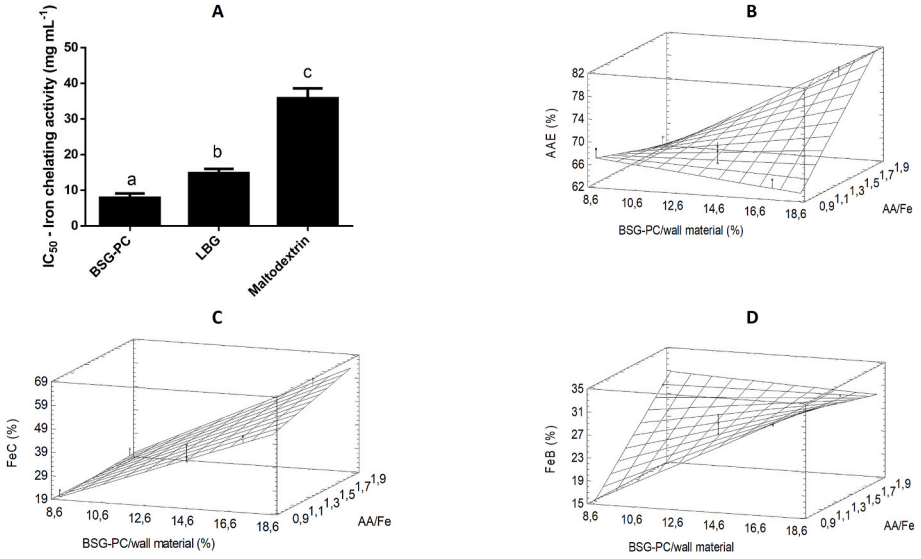

Fig. 2. Iron-chelating activity of BSG-PC, locus bean gum (LBG), and maltodextrin (**A**). Response surface plot corresponding to the effects of BSG-PC/wall material proportion and ascorbic acid/iron molar ratio (AA/Fe) on ascorbic acid encapsulation (AAE) (**B**), iron chelated by the wall material (FeC) (**C**), and iron bioaccessibility (FeB) (**D**). The model of prediction for (**B**), (**C**), and (**D**) was: $y = a_0 + a_1$ BSG-PC/wall material (%) + a_2 AA/Fe + a_3 BSG-PC/wall material (%) x AA/Fe and the corresponding regression coefficients were: a_0, a_1, a_2, and a_3. Different letters in bars mean significant differences between samples ($p < 0.05$).

Table 2
Analysis of variance for the overall effect of the two variables (BSG-PC/wall material and AA/Fe molar ratio) on particle size, iron encapsulation yield (FeE), ascorbic acid encapsulation (AAE), zeta potential, iron chelated by wall material (FeC), iron bioaccessibility (FeB), and surface hydrophobicity of the different microcapsules.

Source of variation	*P-values*[†]						
	Particle size (μm)	FeE (%)	AAE (%)	Zeta potential (mV)	FeC (%)	FeB (%)	Surface hydrophobicity
BSG-PC/wall material (%)	**0.0127**	0.0831	0.0663	**0.0075**	**0.0131**	**0.0398**	**0.0191**
AA/Fe	**0.0234**	**0.0109**	0.0877	0.9507	0.2709	0.0568	0.1337
BSG-PC/wall material (%) x AA/Fe	0.6115	0.2125	**0.0283**	0.7430	0.4500	**0.0433**	0.4527
Lack of fit	0.2457	0.3637	0.1905	0.6840	0.1366	0.7727	0.0865
r^2	0.9247	0.9377	0.8320	0.7947	0.8170	0.9335	0.8271

BSG-PC/wall material (%): proportion of brewers' spent grain protein concentrate respect to total encapsulating material (g 100 g^{-1} encapsulating material). **AA/Fe**: Ascorbic acid/iron molar ratio. [†]Bold values indicate significant differences ($p < 0.05$). Degrees of freedom: n-1.

values of FeE corresponded to the microcapsules obtained with 0.9 AA/Fe molar ratio (Table 1). Similar FeE values (91–97%) were observed for ferrous sulfate encapsulated with chitosan by spray-drying (Singh, Siddiqui, & Diosady, 2018).

In the case of AAE, only the effect of the interaction BSG-PC/wall material x AA/Fe was significant ($p < 0.05$) (Table 2). The value of AAE was higher when AA/Fe molar ratio increased, at the higher BSG-PC/wall material level and when BSG-PC/wall material proportion increased, at the higher AA/Fe level. Then, a maximum in AAE response surface was observed at 17.2% BSG-PC/wall material and 1.8 AA/Fe molar ratio (Fig. 2B). Pierucci, Andrade, Baptista, Volpato, and Rocha-Leão (2006) observed for ascorbic acid encapsulated with pea protein concentrate-maltodextrin blend that AAE increased as pea protein/wall material proportion increased from 50 to 100%. The positive effect of pea protein content on AAE was attributed to an increase of electrostatic interactions between wall material and core. Moreover, the solvation of pea proteins by low MW saccharides provided by maltodextrin (glucose and maltose) reduced the physical-chemical interactions of proteins with AA. Thus, an increase of BSG-PC respect to wall material could favor electrostatic interactions with ascorbic acid, increasing the AAE. In this regard, an increase in BSG-PC/wall material proportion increased negative charge of microcapsules, zeta potential being more negative (Table 1). This may be due to two factors: the high content of Glu + Asp in BSG-PC and the reduction of the content of MD in the formulation. Note that zeta potential of MD is +29.8 (Churio & Valenzuela, 2018). Furthermore, the higher negative charge of microcapsules as the BSG-PC increases would indicate that it is on the surface surrounding AA-Fe complex. This result is very important, since BSG-PC would protect AA-Fe from oxidation by environment, which would favor its reduced state. Note that iron can undergo oxidation, affecting its solubility and therefore its bioavailability (Caetano-Silva et al., 2020). Furthermore, as ascorbic acid is inside the microcapsule it would act as a reducing agent, keeping Fe in its ferrous state. Thus, the main effects of BSG polypeptides and ascorbic acid are to keep the iron soluble at neutral pH (as 6.5 is the pH at duodenum level, the site of iron absorption) and in its reduced state (as ferrous iron).On the other hand, surface hydrophobicity of microcapsules increased proportionally with BSG-PC/wall material proportion (Tables 1 and 2) probably due to the formation of hydrophobic patches.

Fig. 2C shows the iron chelated by the wall material of microcapsules (FeC). Only the effect of BSG-PC/wall material was significant ($p < 0.05$) (Table 2), FeC increasing with BSG-PC ($r^2 = 0.8725$). This result can be due to the high iron-chelating activity of BSG-PC related with the high proportion of 2900 Da polypeptides and chelating amino acid residues (Glu, Asp, and His), which would keep the iron bound. Moreover, this result would indicate that the chelating effect exerted by BSG-PC on iron is higher than that of LGB in the microcapsule, which agrees with the aforementioned (Fig. 2A).

Iron bioaccessibility (FeB) ranged 15.5–30.7% (Table 1). The effects of BSG-PC/wall material and the interaction BSG-PC/wall material x AA/Fe were significant ($p < 0.05$) (Table 2). A maximum in FeB response surface was observed at 17.2% BSG-PC/wall material in all AA/Fe levels (Fig. 2D). However, at low BSG-PC values, FeB increased with the increase of AA/Fe molar ratio. As mentioned before, AA keeps iron in its ferrous state and also acts as chelating agent, favoring iron absorption (Hurrell & Egli, 2010). Thus, at low levels of BSG-PC, AA promote iron bioaccessibility in a dose response way. However, when BSG-PC content is high, it acts as chelating and reducing agent, allowing higher FeB in all AA/Fe molar ratio range. At intestinal pH ferric iron is insoluble, while ferrous iron is still soluble (Bryszewska et al., 2019). Therefore, the high chelating and reducing capacity of BSG-PC could keep the iron soluble and in its reduced state. In this regard, Cian et al. (2016) reported that chelating peptides obtained from red seaweed *Pyropia columbina* hydrolyzates maintained the iron in a soluble and bio-accessible form after gastrointestinal digestion. Moreover, Cian, Drago, De Greef, Torres, and González (2010) observed that peptides produced during hemoglobin proteolysis with commercial proteases increased heme-iron dialyzability. This increase was attributed to chelating peptides that are able to form a soluble iron complex.

3.3. Optimization and model validation

A multiple response optimization of FeE, AAE, FeB, and FeC was performed using the Derringer's desirability function (Fig. 3A). The global desirability function value was 0.7447, and the obtained optimal conditions were 17.2% BSG-PC/wall material and 1.5 AA/Fe molar ratio.

The suitability of the generated mathematical model to predict maximum FeE, AAE, FeB, and FeC was experimentally validated using the conditions determined in the optimization. The experimental values as well as those predicted by the generated mathematical model showed adequate agreement ($p > 0.05$) (Table 3). Fig. 3B shows the morphology of the microcapsules obtained in optimal conditions. Microcapsules had 10.4 ± 0.5 μm and presented round external surfaces with some concavities, typical of spray-dried products (Mohan, Rajendran, He, Bazinetc, & Udenigwe, 2015).

It is important to remark that BSG proteins were obtained from a low cost by-product of brewery. It was possible to use these proteins as encapsulating material with bioactive characteristics. The use of proteins from sources considered wastes could contribute not only to given them a high-added value (Galanakis, 2012), but also to the sustainability of food systems reducing the environmental and economic impacts of food waste (Galanakis, 2020).

The optimization procedure allowed obtaining a fortifier with the higher iron bioaccessibility and iron content. Taking into account that main wall materials are made of soluble components (maltodextrin, LBG, and BSG proteins/polypeptides), and that this may affect the stability of the microcapsule during storage, the potential application of this product is for fortifying powder foods, like dried soups, powders to prepare chocolate drinks, etc.

4. Conclusion

Microcapsules containing iron and ascorbic acid were formulated in

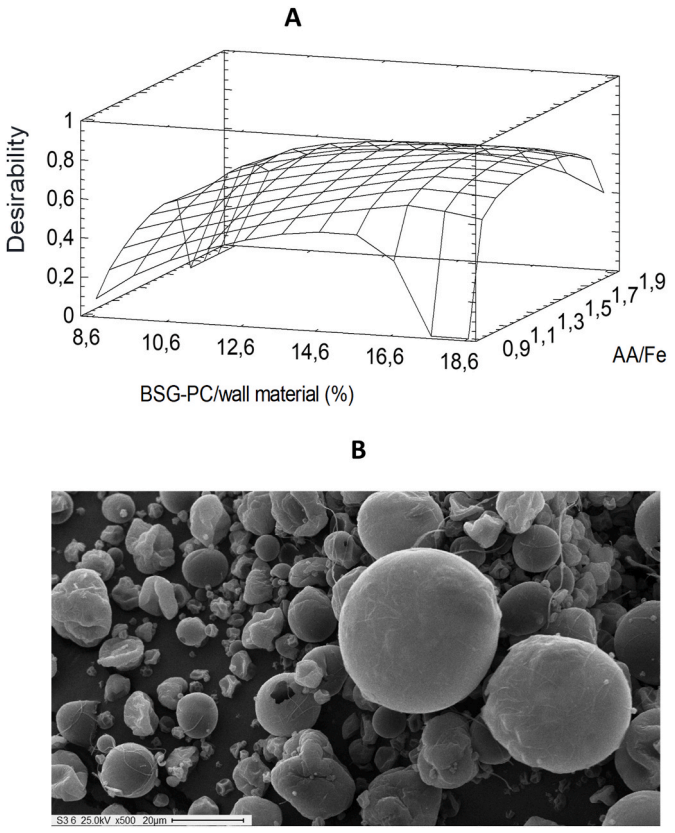

Fig. 3. Multiple responses optimization surface (**A**). Scanning electron micrographs of microcapsules obtained in optimal conditions (BSG-PC/wall material: 17.2 g 100 g^{-1} encapsulating material and AA/Fe: 1.5 M ratio) (**B**).

Table 3
Predicted and experimental mean values of microcapsules obtained in optimal conditions (**BSG-PC/wall material**: 17.2 g 100 g^{-1} encapsulating material and **AA/Fe**: 1.5 M ratio).

Model validation	FeE (%)	AAE (%)	FeC (%)	FeB (%)
Predicted Value[a]	90.6	72.4	53.6	30.2
Experimental value[b]	91.6 ± 2.7	71.3 ± 1.5	52.1 ± 2.3	28.9 ± 2.2

FeE: Iron encapsulation yield. AAE: ascorbic acid encapsulation. FeC: iron chelated by wall material. FeB: iron bioaccessibility.

[a] Values obtained using the polynomial equation ($y = a_0 + a_1$ **BSG-PC/wall material (%)** $+ a_2$ **AA/Fe** $+ a_3$ **BSG-PC/wall material (%)** x **AA/Fe**) and the corresponding regression coefficients (a_0, a_1, a_2, and a_3).

[b] Mean ± standard deviation (n = 3).

order to develop a fortifier with high bioaccessibility protected iron. BSG proteins and polypeptides played an important role as wall material, not only as structural component but also because of it chelating and antioxidant capacity, surrounding iron-ascorbic acid complex, preventing ascorbic acid oxidation during spray drying process and maintaining iron in a soluble form under gastrointestinal tract environment conditions.

The optimization procedure allowed obtaining a fortifier with the higher iron bioaccessibility and iron content, with potential application to powder foods.

Future studies about the effect of this source of iron on food matrix stability (oxidative and organoleptic properties) and the in vivo effects preventing iron deficiency must be performed to evaluate the feasibility of this new microencapsulated fortifying.

Declaration of competing interest

The authors declare that there are no conflicts of interest.

Acknowledgments

REC, JLP, PRS, and SRD carried out the experiment. REC, PRS and SRD analyzed the data and wrote the paper, and had primary responsibility for final content. All authors read and approved the final manuscript. The authors are thankful to the Agencia Nacional de Promoción Científica y Tecnológica (ANPCyT) from Argentina for the financial support through project PICT-2016-2879.

References

Alaiz, M., Navarro, J., Giron, J., & Vioque, E. (1992). Amino acid analysis by high performance liquid chromatography after derivatization with diethylethoxymethylenemalonate. *Journal of Chromatography A, 591*, 181–186.
AOAC. (1995). *Official methods of analysis* (16th ed.). Washigton DC, USA: Horowitz.
Bamdad, F., & Chen, L. (2013). Antioxidant capacities of fractionated barley hordein hydrolysates in relation to peptide structures. *Molecular Nutrition & Food Research, 57*, 493–503.
Bamdad, F., Wu, J., & Chen, L. (2011). Effects of enzymatic hydrolysis on molecular structure and antioxidant activity of barley hordein. *Journal of Cereal Science, 54*, 20–28.
Bryszewska, M. (2019). Comparison study of iron bioaccessibility from dietary supplements and microencapsulated preparations. *Nutrients, 11*, 273.
Bryszewska, M., Tomás-Cobos, L., Gallego, E., Villalba, M., Rivera, D., Taneyo Saa, D., et al. (2019). *In vitro* bioaccessibility and bioavailability of iron from breads fortified with microencapsulated iron. *LWT-Food Science and Technology, 99*, 431–437.
Caetano-Silva, M., Netto, F., Bertoldo-Pacheco, M., Alegría, A., & Cilla, A. (2020). Peptide-metal complexes: Obtention and role in increasing bioavailability and decreasing the pro-oxidant effect of minerals. *Critical Reviews in Food Science and Nutrition*. https://10.1080/10408398.2020.1761770.
Celus, I., Brijs, K., & Delcour, J. (2007). Enzymatic hydrolysis of brewers' spent grain proteins and technofunctional properties of the resulting hydrolysates. *Journal of Agricultural and Food Chemistry, 55*, 8703–8710.
Churio, O., & Valenzuela, C. (2018). Development and characterization of maltodextrin microparticles to encapsulate heme and non-heme iron. *LWT-Food Science and Technology, 96*, 568–575.
Cian, R., Drago, S., De Greef, M., Torres, R., & González, R. (2010). Iron and zinc availability and some physical characteristics from extruded products with added concentrate and hydrolysates from bovine hemoglobin. *International Journal of Food Sciences & Nutrition, 61*, 573–582.
Cian, R., Garzón, A., Betancur-Ancona, D., Chel-Guerrero, L., & Drago, S. (2015). Hydrolyzates from *Pyropia columbina* seaweed have antiplatelet aggregation, antioxidant and ACE I inhibitory peptides which maintain bioactivity after simulated gastrointestinal digestion. *LWT-Food Science and Technology, 64*, 881–888.
Cian, R., Garzón, A., Betancur-Ancona, D., Chel-Guerrero, L., & Drago, S. (2016). Chelating properties of peptides from red seaweed *Pyropia columbina* and its effect on iron bio-accessibility. *Plant Foods for Human Nutrition, 71*, 96–101.
Cian, R., Garzón, A., Martínez-Augustín, O., Botto, C., & Drago, S. (2018). Antithrombotic activity of Brewers' spent grain peptides and their effects on blood coagulation pathways. *Plant Foods for Human Nutrition, 73*, 241–246.
Cian, R., Salgado, P., Mauri, A., & Drago, S. (2020). *Pyropia columbina* phycocolloids as microencapsulating material improve bioaccessibility of brewers' spent grain peptides with ACE-I inhibitory activity. *International Journal of Food Science and Technology, 55*, 1311–1317.
Conolly, A., Piggott, C., & FitzGerald, R. (2014). Technofunctional properties of a brewers' spent grain protein-enriched isolate and its associated enzymatic hydrolysates. *LWT-Food Science and Technology, 59*, 1061–1067.
Derringer, G., & Suich, J. (1980). Simultaneous optimization of several response variables. *Journal of Quality Technology, 12*, 214–219.
Drago, S., Binaghi, M., & Valencia, M. (2005). Effect of gastric digestion pH on iron, zinc and calcium availability from preterm and term starting infant formulas. *Journal of Food Science, 70*, 107–112.
Galanakis, C. (2012). Recovery of high added-value components from food wastes: Conventional, emerging technologies and commercialized applications. *Trends in Food Science & Technology, 26*, 68–87.
Galanakis, C. (2020). The food systems in the era of the Coronavirus (COVID-19) pandemic crisis. *Foods, 9*, 523.
Gharibzahedi, S., & Jafari, S. (2017). The importance of minerals in human nutrition: Bioavailability, food fortification, processing effects and nanoencapsulation. *Trends in Food Science & Technology, 62*, 119–132.
Gupta, C., Chawla, P., Arora, S., Tomar, S., & Singh, A. (2015). Iron microencapsulation with blend of gum Arabic, maltodextrin and modified starch using modified solvent evaporation method—milk fortification. *Food Hydrocolloids, 43*, 622–628.
Hamdani, A., & Wani, I. (2017). Guar and Locust bean gum: Composition, total phenolic content, antioxidant and antinutritional characterization. *Bioactive Carbohydrates and Dietary Fibre, 11*, 53–59.
Huang, Tao, L., Zhang, Fan, & Yong. (2019). Synthesis and characterization of an antioxidative galactomannan–iron(III) complex from *Sesbania* seed. *Polymers, 11*, 28.

Hurrell, R., & Egli, I. (2010). Iron bioavailability and dietary reference values. *American Journal of Clinical Nutrition, 91*, 1461S–1467S.

Lazarte, C., Carlsson, N., Almgren, A., Sandberg, A., & Granfeldt, Y. (2015). Phytate, zinc, iron and calcium content of common Bolivian food, and implications for mineral bioavailability. *Journal of Food Composition and Analysis, 39*, 111–119.

Lv, Y., Liu, Q., Bao, X., Tang, W., Yang, B., & Guo, S. (2009). Identification and characteristics of iron-chelating peptides from soybean protein hydrolysates Using IMAC-Fe^{3+}. *Journal of Agricultural and Food Chemistry, 57*, 4593–4597.

McCarthy, A., O'Callaghan, Y., Connolly, A., Piggott, C., FitzGerald, R., & O'Brien, N. (2013). *In vitro* antioxidant and anti-inflammatory effects of brewers' spent grain protein rich isolate and its associated hydrolysates. *Food Research International, 50*, 205–212.

Miller, D., Schricker, B., Rasmussen, R., & Van Campen, D. (1981). An *in vitro* method for estimation of iron availability from meals. *American Journal of Clinical Nutrition, 34*, 2248–2256.

Mohan, A., Rajendran, S., He, Q., Bazinetc, L., & Udenigwe, C. (2015). Encapsulation of food protein hydrolysates and peptides: A review. *RSC Advances, 5*, 79270–79278.

Molina-Ortiz, S., Mauri, A., Monterrey-Quintero, E., Trindade, M., Santana, A., & Favaro-Trindade, C. (2009). Production and properties of casein hydrolysate microencapsulated by spray drying with soybean protein isolate. *LWT-Food Science and Technology, 42*, 919–923.

Moslemi, M., Hosseini, H., Erfan, M., Mortazavian, A., Mazaheri, R., Neyestani, T., et al. (2014). Characterisation of spray-dried microparticles containing iron coated by pectin/resistant starch. *International Journal of Food Science and Technology, 49*, 1736–1742.

Moslemi, M., Hosseini, H., Neyestani, T., Akramzadeh, N., & Mazaheri, N. (2018). Effects of non-digestive polymers used in iron encapsulation on calcium and iron apparent absorption in rats fed by infant formula. *Journal of Trace Elements in Medicine & Biology, 50*, 393–398.

Nesterenko, A., Alric, I., Silvestre, F., & Durrieu, V. (2013). Vegetable proteins in microencapsulation: A review of recent interventions and their effectiveness. *Industrial Crops and Products, 42*, 469–479.

Norkaew, O., Thitisut, P., Mahatheeranont, S., Pawin, B., Sookwong, P., Yodpitak, S., et al. (2019). Effect of wall materials on some physicochemical properties and release characteristics of encapsulated black rice anthocyanin microcapsules. *Food Chemistry, 294*, 493–502.

Oliveira, A., Moretti, T., Boschini, C., Baliero, J., Freitas, A., Freitas, O., et al. (2007). Microencapsulation of B. lactis (BI 01) and L. acidophilus (LAC 4) by complex coacervation followed by spouted-bed drying. *Drying Technology, 25*, 1687–1693.

Palacios, S. (2012). Ferrous versus ferric oral iron formulations for the treatment of iron deficiency: A clinical overview. *The ScientificWorld Journal*, 846824, 2012.

Pierucci, A., Andrade, L., Baptista, E., Volpato, N., & Rocha-Leão, M. (2006). New microencapsulation system for ascorbic acid using pea protein concentrate as coat protector. *Journal of Microencapsulation, 23*, 654–662.

Proaño, J., Salgado, P., Cian, R., Mauri, A., & Drago, S. (2020). Physical, structural and antioxidant properties of brewer's spent grain protein films. *Journal of the Science of Food and Agriculture*. https://doi.org/10.1002/jsfa.10597

Roman, M., Decker, E., & Goddard, J. (2015). Performance of nonmigratory iron chelating active packaging materials in viscous model food systems. *Journal of Food Science, 80*, 1965–1973.

Sassi, C., Marcet, I., Rendueles, M., Díaz, M., & Fattouch, S. (2020). Egg yolk protein as a novel wall material used together with gum Arabic to encapsulate polyphenols extracted from *Phoenix dactylifera* L pits. *Lebensmittel-Wissenschaft und -Technologie-Food Science and Technology, 131*. https://doi.org/10.1016/j.lwt.2020.109778

Singh, A., Siddiqui, J., & Diosady, L. (2018). Characterizing the pH-dependent release kinetics of food-grade spray drying encapsulated iron microcapsules for food fortification. *Food and Bioprocess Technology, 11*, 435–446.

Torres-Fuentes, C., Alaiz, M., & Vioque, J. (2011). Affinity purification and characterization of chelating peptides from chickpea protein hydrolysates. *Food Chemistry, 129*, 485–490.

Van de Velde, F., Pirovani, M., Cámara, M., Güemes, D., & Bernardi, C. (2012). Optimization and validation of a UV–HPLC method for vitamin C determination in strawberries (*Fragaria ananassa* Duch.), using experimental designs. *Food Analytical Methods, 5*, 1097–1104.

Vieira, E., Angélica, M., Rocha, M., Coelho, E., Pinho, O., Saraivab, J., et al. (2014). Valuation of brewer's spent grain using a fully recyclable integrated process for extraction of proteins and arabinoxylans. *Industrial Crops and Products, 52*, 136–143.

Vieira, E., Teixeira, J., & Ferreira, I. (2016). Valorization of brewers' spent grain and spent yeast through protein hydrolysates with antioxidant properties. *European Food Research and Technology, 242*, 1975–1984.

Wang, C., Chang, S., Inbaraj, B., & Chen, B. (2010). Isolation of carotenoids, flavonoids and polysaccharides from *Lycium barbarum* L. and evaluation of antioxidant activity. *Food Chemistry, 120*, 184–192.

Xie, Y., Wan, A., Lu, Q., & Hui, M. (2010). The effects of rheological properties of wall materials on morphology and particle size distribution of microcapsule. *Czech Journal of Food Sciences, 28*, 433–439.

Yang, S., Mao, X., Li, F., Zhang, D., Leng, X., Ren, F., et al. (2012). The improving effect of spray-drying encapsulation process on the bitter taste and stability of whey protein hydrolysate. *European Food Research and Technology, 235*, 91–97.

Yang, L., Zhang, Y., Wang, J., Huang, Z., Gou, L., Wang, Z., et al. (2016). Non-heme iron absorption and utilization from typical whole Chinese diets in young Chinese urban men measured by a double-labeled stable isotope technique. *PloS One, 11*, Article e0153885.